Exfoliated MoS<inf>2</inf> Nanosheet/Cellulose Nanocrystal Flexible Composite Films as Electrodes for Zinc Batteries

ACS APPLIED NANO MATERIALS

www.acsanm.org

Article

Exfoliated MoS_2 Nanosheet/Cellulose Nanocrystal Flexible Composite Films as Electrodes for Zinc Batteries

Amit Kumar Sonker,* Shizhao Xiong, Ruchi Aggarwal, Martina Olsson, Arnita Spule, Seyedehsan Hosseini, Sumit Kumar Sonkar, Aleksandar Matic, and Gunnar Westman*

Cite This: *ACS Appl. Nano Mater.* 2023, 6, 8270−8278

Read Online

ACCESS | Metrics & More | Article Recommendations | Supporting Information

ABSTRACT: The study presents a more efficient way of exfoliating MoS_2 in water and the exfoliated MoS_2 was used in an electrode. The electrodes were prepared from exfoliated MoS_2 (active material)−nanocrystalline cellulose (binder) with carbon nanotubes (electron-conducting support) and demonstrated in a zinc battery half-cell that showed a Coulombic efficiency of 90%. Successful exfoliation of MoS_2 was done by sonication of bulk MoS_2 with sulfated cellulose nanocrystals (CNC) for 4 h. The exfoliation was confirmed by Raman and transmission electron microscopy; interestingly, the Raman signals for exfoliated MoS_2 show a blue shift for both A_{1g} and E^1_{2g} bands, which may be an indication of an induced lattice strain effect from the CNC on MoS_2. The resulting stable water suspension showed no tendency of precipitation after 2 months of standing. The zeta potential, ζ, for sodium sulfated CNC (CNC−OSO_3Na)−MoS_2 in water suspension was −45 mV, whereas sulfated CNC (CNC−OSO_3H)−MoS_2 in water suspension had a zeta potential of −35 mV. The sodium form of sulfated CNCs displayed micelle characteristics, similar to sodium dodecyl sulfate (SDS), with a critical aggregation concentration (CAC) of 1.1 wt %. At CAC, the CNCs efficiently exfoliated MoS_2, which is at a much lower concentration than has been reported for synthetic surfactants like SDS and cetyl trimethyl ammonium bromide.

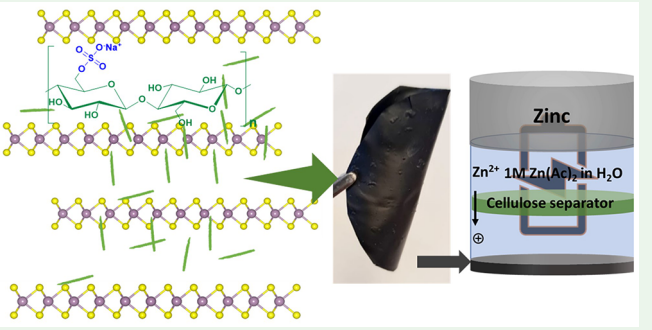

KEYWORDS: *cellulose nanocrystals, two dimensional (2D) nanomaterials, exfoliation, critical aggregation concentration, biobased surfactants, composite, electrode, Zn battery (half-cell)*

1. INTRODUCTION

Transition metal dichalcogenides (TMDs) are an emerging class of two-dimensional (2D) nanomaterials. TMDs are denoted by the formula MX_2, where X belongs to the chalcogenide family and M belongs to transition metal of group IV, V, and VI, such as MoS_2, WS_2, $MoSe_2$, WSe_2, and so forth.[1] Owing to the properties of TMDs, particularly to MoS_2, they have gained attention for application in high-performance supercapacitors,[2] small biomolecule sensors,[3] Li-ion batteries,[4] and visible light photocatalysis.[5] However, multilayers of MoS_2 do not perform well in electrochemical applications due to low conductivity, high volumetric strain, and aggregation during the cycling and drying of electrode material.[4] On the other hand, ultra-thin layers of MoS_2 have unique properties suitable for application in supercapacitors,[6] batteries,[7] detectors,[8] hydrogen evolution reactions,[9] potent adsorbent material for wastewater treatment,[10] field-effect transistors,[11] and sliding lubricant[12] which saves energy and increases service life. In addition to the energy applications, a few layers of MoS_2 also have potential as reinforcing agents in polymer composites.[13]

Consequently, there has been research and development of efficient methods to form stable nanosheets from TMDs. Exfoliation of bulk MoS_2 is an established methodology to obtain MoS_2 nanosheets. Two of the more common exfoliation techniques are mechanical exfoliation (ME)[14] and liquid-phase exfoliation (LPE).[15,16] ME is well known to obtain monolayer and few-layer MoS_2. Major drawbacks are the low yield, and reaggregation of exfoliated sheets with the substrates restricts its applicability. Therefore, LPE is commonly used to exfoliate TMD on a large scale (kilograms). In LPE, TMDs are mixed and directly ultrasonicated in organic solvents (*N*-methyl pyrrolidone[16,17] and dimethylformamide[18]). However, these solvents are toxic and have a high boiling point, in comparison to other common organic solvents, which may make sheets restack due to slow solvent evaporation, so even though the process works, it lacks both techno and economical features to

Received: February 6, 2023
Accepted: April 28, 2023
Published: May 15, 2023

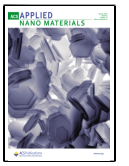

be scaled and lacks perspectives of being a green chemical process.[16]

To improve exfoliation and aspire for green process metrics, additives like polymers[19] and surfactants [sodium dodecyl sulfate (SDS),[20] sodium cholate,[21] and cetyl trimethyl ammonium bromide (CTAB)[20] have been added to suitable solvents to make the sonication process more efficient. However, the surfactants are added in excess, and removal of non-interacting surfactant molecules is difficult, and the residual amount attached to the surface of TMD sheets affects its properties. Consequently, this methodology has not received any major impact, especially for the use of TMDs in biological and biosensing applications. Recently, ammonia,[22] ATP,[23] lignin,[24] and bovine serum albumin[13,25] have been reported as effective exfoliating agents to induce the exfoliation of TMDs. However, using biomacromolecules and biopolymers as exfoliating agents to disperse MoS_2, there is a possibility that they fold or surround the surface of TMD, thereby limiting the applications.[23]

Herein, we present the preparation of water-stable suspensions of MoS_2 nanosheets by one-step exfoliation using sulfated cellulose nanocrystals (CNC). A few reports are already available where cellulose nanofibrils (CNF) have been used in dispersing MoS_2 to prepare nanosheets used for energy storage devices[4,26] and fire retardant aerogels.[27] In comparison, CNCs are the most crystalline form of nanocellulose and have lower viscosity and higher charge density than CNF at the same dry content. In this work, CNCs are used as surfactants and exfoliating agents, leading to a more efficient extraction, 34 wt % of MoS_2 compared to 21 wt % when extracted by CNF,[4] which is the novelty of the presented work. They are prepared from microcrystalline cellulose (MCC) by sulfuric acid hydrolysis, yielding CNCs with sulfate groups on the surface (CNC−OSO_3H) that exhibit very good dispersibility in water. By ion exchange, they are converted into the sodium sulfated form of CNC (CNC−OSO_3Na). The replacement of hydrogen with sodium in the sulfate groups results in higher heat stability and dispersibility compared to CNC−OSO_3H, and the sodium form of CNC starts to form gels at a lower concentration than CNC−OSO_3H does. It was assumed that a concentration close to the critical aggregation concentration (CAC) was needed for efficient exfoliation of MoS_2. Thus, first, the zeta potential and CAC for CNC−OSO_3Na were determined. Successful exfoliation was verified by transmission electron microscopy (TEM), X-ray diffraction (XRD), and Raman. To demonstrate the applicability of the exfoliated nanosheets, a stable formulation of CNC, MoS_2, and multi-walled carbon nanotube (MWCNT) was used to prepare a composite electrode material. The new exfoliated MoS_2−CNC film was evaluated in a Zn half-cell as a substrate for the electrodeposition of Zn to demonstrate its capability of stable cycling and the potential application as a current collector of the anode in Zn metal batteries. Therefore, our work also shows great promise of the application of this exfoliated MoS_2-based composite in a sustainable, environmentally friendly, and low-cost energy storage system.

2. MATERIALS AND METHODS

2.1. Materials. MoS_2 (98%, particle size < 2 μm), sulfuric acid (99%), MCC (from cotton linters) (Avicel PH-101), SDS, sodium hydroxide, zinc foil (thickness of 0.25 mm, 99.9% trace metals basis), and zinc acetate [$Zn(OAc)_2$, 99.99% trace metals basis] were purchased from Sigma-Aldrich (USA). MWCNTs and cellulose separator (TF4050) were purchased from Suzhou Tanfeng Graphene Technology Co., Ltd. and Nippon Kodoshi Corporation, respectively.

2.2. Methods. *2.2.1. Preparation of CNC from MCC.* As described earlier,[28,29] CNCs were prepared by acid hydrolysis of MCC. Acid hydrolysis was performed by mixing 40 g of MCC in 64% sulfuric acid solution (710 mL) preheated to 45 °C for 2 h. After heating, the mixture was transferred into deionized (DI) water (7 L) to stop cellulose's further hydrolysis by acid. The whole mixture was centrifuged using Thermo Scientific Heraeus Megafuge 40 centrifuge equipped with a TX-750 high versatility swinging bucket rotor at 4031*g* RCF to remove water, and the CNC was recovered at the bottom of centrifuge tubes in paste form. The CNC was redispersed in water, approx. 1 L, and subjected to dialysis using Spectra/Por molecular porous membrane tubing, 7 MWCO, 12−14 kDa, against water to remove unreacted acid impurities. The water was regularly changed in 12 h intervals until a conductivity of <5 μS was obtained. The CNC water suspension was sonicated to remove big lumps of unhydrolyzed cellulose. The samples were stored in a refrigerator at 4 °C in suspension form with a dry content of 2 wt %. The obtained CNCs were well dispersed in water, pH ∼ 3.0, due to sulfate groups. The acid hydrolysis results in the formation of sulfate groups to some of the hydroxyl groups. The ion exchange was performed in a 1:1 mol equivalent reaction with NaOH according to the number of sulfate half ester groups available on CNC surfaces. The CNC had a 285 ± 7 μmol/g sulfate half-ester group content for this batch, determined by conductometric and potentiometric titration. All details are given in Supporting Information.

2.2.2. Determination of CAC of Sulfated CNC Samples. The critical aggregation concentration (CAC) of CNCs was determined by conductometry,[30,31] similar to determining critical micelle concentrations (CMC) for commercial surfactants like SDS and CTAB. A stock solution of 3.5 wt % CNCs obtained from ion exchange with NaOH of sulfated CNCs (SCNCs; H^+ as counter ions replaced by Na^+), CNC−OSO_3Na (S_{Na}CNC), was diluted with DI water in 0.5 mL volumes at regular intervals, and the conductivity of the suspension was regularly monitored.

2.2.3. Exfoliation of MoS_2 in Water Using CNC. Exfoliation of MoS_2 in DI water was performed by using a Sonics Vibra-Cell 500 W sonicator equipped with a standard probe with a tip diameter of 13 mm operating at 40% of maximum amplitude. 2.5 g of MoS_2 powder was added to 60 mL of 1.1 wt % S_{Na}CNC (275 mg dry mass)−DI water suspension. Afterward, the mixture was sonicated for 4 h using a cyclic program of 20 min sonication and 10 min cooling. After sonication, the S_{Na}CNC−MoS_2 samples were centrifuged at 4300 rpm to remove unexfoliated MoS_2 from the suspensions. The samples were monitored daily to check the stability of the suspensions. Even though it is well known in the CNC community that sulfate groups of SCNC are labile, decompose at approximately 90 °C, and are cleaved from the CNC surface by sonication, we initially investigated both SCNCs as well as S_{Na}CNC and their exfoliation efficiency. As expected, when running a control sample of SCNCs, under similar preparation conditions, the high temperature when the ultrasonication method was carried out resulted in desulfation of SCNCs. Consequently, the major work herein is on S_{Na}CNC.

2.2.4. Fabrication of Flexible Composite Film. For preparing a thin composite film, MWCNTs were added to a suspension of active material (MoS_2) and binder (S_{Na}CNC), and the mixture was further sonicated, followed by vigorous stirring to ensure the uniform dispersion of MWCNTs in the suspension. After mixing, the suspension was transferred to a polystyrene Petri dish and kept in a hot air oven at 45 °C overnight for drying. The thickness of the dried film was 90−100 μm, determined by a digital Mitutoyo micrometer. Throughout the article, the prepared film, a composite film, has a composition of exfoliated MoS_2 + S_{Na}CNC + CNT.

2.2.5. Fabrication of a Battery Cell. Zn foil and CNC−MoS_2 composite film were punched into disks with 10 and 14 mm diameters, respectively. The cellulose separator was cut with a diameter of 16 mm, and the electrolyte was prepared by dissolving $Zn(OAc)_2$ in DI water to a concentration of 1 M. A Zn disk and CNC−MoS_2 film sandwiched a cellulose separator soaked with 60 μL

https://doi.org/10.1021/acsanm.3c00543
ACS Appl. Nano Mater. 2023, 6, 8270−8278

Scheme 1. Stepwise Demonstration of the Presented Work

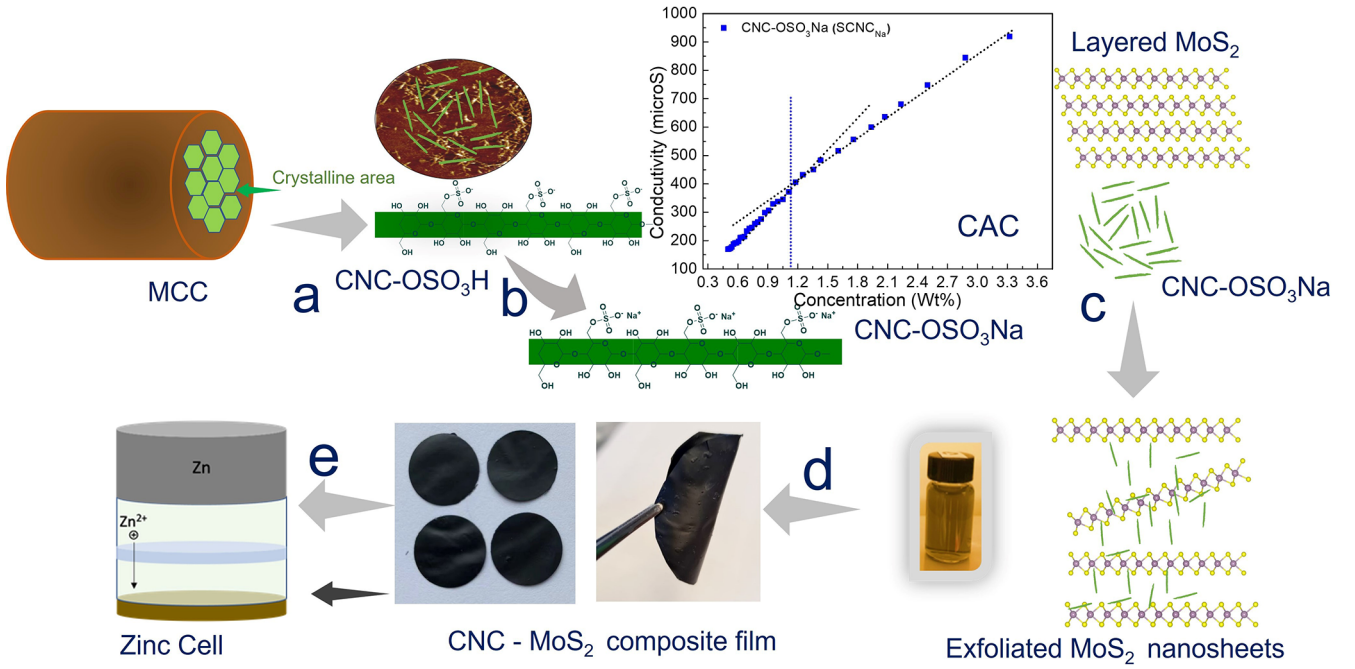

electrolyte and assembled in a CR2032 type coin cell to form a Zn half-cell.

3. CHARACTERIZATION OF SAMPLES

3.1. Raman Spectra. Raman spectra were recorded on a WITec alpha300 Raman spectrometer with a 532 nm laser line. For Raman analysis, samples were prepared by drop-casting aqueous solutions of S_{Na}CNC and S_{Na}CNC−MoS_2 on glass slides and dried in a hot air oven at 40−50 °C. For MoS_2, the powder was placed on the surface of the glass slide and firmly pressed for a homogeneous consistency.

3.2. Atomic Force Microscopy. Atomic force microscopy (AFM) was performed in tapping mode by a multimode scanning probe microscope (Bruker).

3.3. Transmission Electron Microscopy. TEM was performed using a Tecnai G2 20 (FEI) S-Twin model at 200 kV to examine the arrangement of MoS_2 nanosheets. For sample preparation, the S_{Na}CNC−MoS_2 aqueous dilute solution was ultra-sonicated for 30 min. A drop of the diluted solution was then placed on the carbon-coated copper grid surface and dried under air.

3.4. X-ray Diffraction. XRD measurements were performed on a Bruker D8 Advance instrument in the range of 10−50° using scan rate 0.5 s/step using Cu Kα—1.54 Å. The samples were placed on a silicon single crystal sample holder.

3.5. Zeta Potential. Zeta potential (ζ) was measured on a Malvern Zetasizer Nano instrument for SCNC, S_{Na}CNC, and S_{Na}CNC−MoS_2 samples by placing the 0.1 wt % suspensions in the cuvette and measuring in sextuplicate.

3.6. Thermomechanical and Morphological Characterization of a Composite Film. The mechanical properties of films were measured by a universal testing machine from Instron. The electrode film was cut in the form of rectangular strips as per ASTM D 882-12 standard and tested at a 5 mm/min strain rate. The thermal stability of films was measured by thermogravimetric analysis (TGA) using 3+ Star System from Mettler Toledo in the temperature range 25−500 °C under nitrogen gas. Cross-sectional morphology of composite films was imaged on an Ultra 55 FEG scanning electron microscope at 10 keV.

3.7. Electrochemical Characterization of a Battery Cell. Galvanostatic cycling of coin cells was performed on a Scribner 585 battery testing system. The plating and stripping of Zn on the CNC−MoS_2 film was conducted under a current density of 0.5 mA cm^{-2} for 1 h each. The cut-off voltage for stripping was set to 0.6 V. The Coulombic efficiency was defined as the ratio of total stripping capacity to the prior plating capacity.

4. RESULTS AND DISCUSSION

As an overview, the design of the presented work is shown in Scheme 1. (a) SCNCs are prepared by acid hydrolysis of MCC and exhibit high dispersibility in water. Further, to utilize SCNCs as an exfoliating agent to disperse MoS_2 in water (b), the SCNC has to be converted to S_{Na}CNC by an ion-exchange reaction to obtain CNC's with higher thermal stability since the sonication treatment generates heat that desulfate the CNC.[32] (c) The S_{Na}CNC (CNC−OSO_3Na) samples had a CAC of 1.1 wt % determined by the conductometry method and were used to exfoliate layered bulk MoS_2 material into nanosheets by ultrasonication. (d) For application, the combination of MoS_2 and CNC and MWCNT is used to prepare a free-standing flexible composite (e) as an electrode tested in a Zn half-cell.

The stability of SCNC and S_{Na}CNC in water can be predicted from zeta-potential measurement. Particles with a value higher than +30 mV or below −30 mV usually has a good water stability. Apart from giving water stability to the sulfate groups, the charge on the CNC surface affects how CNC forms aggregates in water and affects their CAC. For surfactants like SDS, the CMC is commonly determined by adding a surfactant and plotting conductivity as a function of concentration. There is a change in the conductivity at CMC due to different degrees of accessible SDS that can be ionized

https://doi.org/10.1021/acsanm.3c00543
ACS Appl. Nano Mater. 2023, 6, 8270−8278

below and above CMC (Figure S2a in Supporting Information). On the other hand, if a highly concentrated suspension is diluted, the conductivity decreases due to inclusion of ions of opposite charge (counterions) to the long-chain ions within the micelle. When CMC is reached, the conductivity starts to decrease more rapidly due to the independent contribution of anions $[CH_3(CH_2)_{11}-OSO_3^-]$ and cations (Na^+).[31] The point of intersection of the two different trends of conductivity is considered a CMC for SDS (8 mM). Similarly, CAC can be determined for amphiphilic particles. CNC particles can be considered amphiphilic, at least the CNCs from the cotton source, for which it is generally accepted that the CNCs have a hexagonal cross-section, wherein four faces are hydrophilic and two opposite phases are hydrophobic.[33] However, it shall be stressed that there is no consensus on the exact cross-section of cellulose; different sources may have different fibrillar cross-sections. Notwithstanding this, we expect that the CNC can act like a surfactant. A 3.5 wt % CNC water suspension was diluted with 0.5 mL portions in regular intervals, and the conductivity was plotted as a function of concentrations [Figure S2b in Supporting Information]. The conductivity of S_{Na}CNC suspension reduced upon dilution and gave a clear change in slope at 1.1 wt %, determined as the CAC concentration. At first, it may be expected that the crystallites become more dispersed and mobile upon dilution, and consequently, more sulfate groups become available for detection, and the conductivity should increase. However, due to solvation and decreasing ionic strength (inclusion of charges of different ions within CNC) between S_{Na}CNC, a decreasing trend in conductivity is observed instead of increasing. As CAC is reached, the slope of the conductivity curve gradually decreases since the conductivity due to solvated S_{Na}CNC at lower concentrations is expected to be relatively less mobile. The point of intersection of two different decreasing conductivity trends is assigned as the CAC for the S_{Na}CNC samples [Figure S2b]. The CAC was found to be 1.1 wt %.

To correlate the CAC to the surface charge and get indications on the colloidal stability, the zeta potential of the samples were measured. Zeta potential gives surface charge and provides guidance on the colloidal stability of suspensions of nanomaterials. It is considered that particles with zeta potentials above +30 mV or below −30 mV are considered to form stable dispersions due to electrostatic repulsion between nanoparticles.[20] SCNCs have a negative zeta potential of −61 mV in the studied samples with a pH value of 3 and shows excellent water dispersibility due to strong electrostatic repulsion between the sulfate group. Upon ion exchange with NaOH, the S_{Na}CNC samples gets a zeta potential of −50 mV. The difference in the zeta potential between the two samples is due to a decrease in the electrostatic repulsion between the sulfates group upon introducing Na as a counter ion. Both samples, SCNC and S_{Na}CNC, were used to disperse MoS_2 in water, and the stability of the MoS_2−water suspension was measured [Figure 1a,b]. The zeta potential for S_{Na}CNC−MoS_2 in water suspension is observed to be −45 mV, and that for SCNC−MoS_2 in water suspension is −35 mV. Further, to demonstrate the stability of suspensions for a longer time without precipitation, the zeta potential measurement was performed again after 2 months and gave results that are of the same order, indicating similar concentrations and no precipitation. Thus, for the SCNC system, the zeta potential is changed from −61 to −35 mV during the exfoliation,

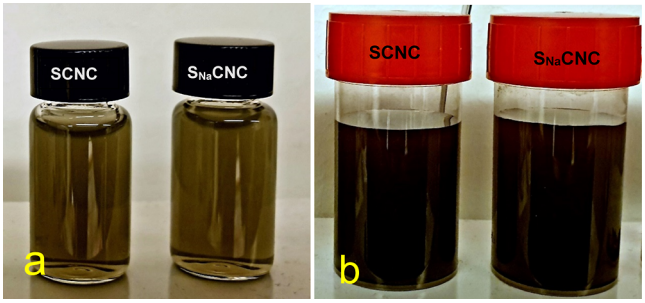

Figure 1. (a) Stability of MoS_2 in water with SCNC (left) and S_{Na}CNC samples (right) in 10 mL vial (samples prepared for zeta-potential measurements of 0.1 wt % concentration). (b) Stability of 1 wt % MoS_2 in water with SCNC (left) and S_{Na}CNC samples (right) in 50 mL vial.

whereas for the S_{Na}CNC systems, a change from −50 to −45 mV is found, showing that sodium as a counter ion makes the sulfate half ester less prone to degradation. Though the stability of MoS_2 in water with both the SCNC and S_{Na}CNC is considered good according to ζ values, the main advantage with S_{Na}CNC samples is a neutral suspension, whereas for SCNC, the suspension is acidic. Furthermore, S_{Na}CNC is much more stable than SCNC.

Sodium ions reduced the electrostatic repulsion between S_{Na}CNC crystals, and hence, its zeta potential is greater than that of SCNC samples. Conceiving this, the stability of MoS_2−S_{Na}CNC suspension increases, and it shows excellent stability in water and behaves like a surfactant molecule, like SDS, and forms aggregates at a concentration of 1.1 wt % (Supporting Information). The hydrophobic part of S_{Na}CNC can interact with hydrophobic MoS_2 basal planes and impart dispensability in water, similar to other examples where cationic and anionic surfactants form stable MoS_2−water suspension.[20]

Further, to confirm exfoliation of MoS_2, CNC samples were characterized by Raman, XRD, and microscopy. Raman spectra of bulk MoS_2 show two optical phonon modes; the E^1_{2g} (382 cm^{-1}) band corresponds to in-plane vibration of two opposite S atoms attached to a Mo atom, and the A_{1g} (408 cm^{-1}) band is related to the out-of-plane vibration of S atoms in opposite directions [Figure 2a].[34] Moreover, in reports by Van Thanh et al.[35] and Zhu et al.,[36] the E^1_{2g} and A_{1g} bands for bulk MoS_2 are located at 376 and 403 cm^{-1}, respectively. This difference is explained in Raman spectroscopic studies published by Windom et al.,[38] where it is suggested that the positions of the E^1_{2g} and A_{1g} bands depend on the bulk source of MoS_2, whether it is a natural crystalline form (molybdenite) or powder form (used in this work). Most of the reports[37] where E^1_{2g} and A_{1g} bands for bulk MoS_2 from molybdenite are located at 381−382 and 406−407 cm^{-1}. However, in addition to this report, for powder samples purchased from Acros,[38] Alfa Aesar,[36] and Sigma-Aldrich (product number 234842), the E^1_{2g} and A_{1g} bands for bulk MoS_2 are located at 375−376 and 402−403 cm^{-1} [Figure 2b].

The intensities, widths, and peak frequencies of E^1_{2g} and A_{1g} bands depend on the thickness (number of layers) of MoS_2 flakes. In most reports, the gap narrowing between the two bands (E^1_{2g}—381 cm^{-1}) and (A_{1g}—406 cm^{-1}) indicates the exfoliation of MoS_2, and the difference between them predicts the number of MoS_2 layers, as reported by Li et al.[34] Moreover, in a few reports, based on the quality of bulk MoS_2, the E^1_{2g} and A_{1g} peaks are observed at 375 and 402 cm^{-1}, respectively. After

https://doi.org/10.1021/acsanm.3c00543
ACS Appl. Nano Mater. 2023, 6, 8270−8278

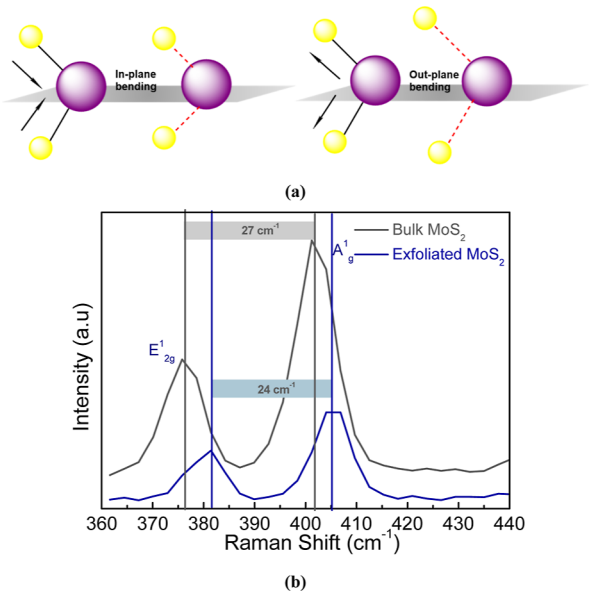

Figure 2. (a) Demonstration of in-plane vibration (E^1_{2g}) of two opposite S atoms attached to a Mo atom and the out-of-plane vibration (A_{1g}) of S atoms in opposite directions. (b) Raman spectra for bulk MoS_2 (powder from Sigma-Aldrich) and exfoliated MoS_2 nanosheets MoS_2–S_{Na}CNC suspension. MoS_2–SCNC suspension shows similar Raman as MoS_2–S_{Na}CNC suspension (see Supporting Information).

exfoliation, instead of coming closer to each other, both bands shift to higher wave numbers, 381 cm^{-1} (E^1_{2g}) and 405 cm^{-1} (A_{1g}).[34] In the present study, a similar observation is made. Instead of decreasing the separation between E^1_{2g} and A_{1g} bands, there is a blue shift of both the bands. However, the shift of the A_{1g} band is not the same as for the E^1_{2g}; the difference between the bands is 24.5 cm^{-1} compared to bulk MoS_2 (27 cm^{-1}). This may be due to lattice strain effect induced on the MoS_2 nanosheets upon the interaction of CNC with MoS_2 sheets, similar to the phenomena described by Yang et al.[39] The S_{Na}CNC and SCNC strongly interact with the basal plane of MoS_2 nanosheets, as explained by the change in zeta potential and apply relatively more strain in-plane than the out-plane. It is explained by Yang et al. that under the in-plane lattice strain, simulated Raman spectra show a shift in E^1_{2g} and A_{1g} band of the same order.

The XRD patterns for MoS_2 bulk powder, exfoliated MoS_2, and the composite film are presented in Figure 3. The bulk MoS_2 shows the characteristic diffraction pattern with peaks at 2θ—14.4° (002 plane), 29° (004 plane), 32.6° (001), 33.4° (101), 35.6° (102), 39.6° (103), and 44.1° (006), and 49.5° (105), according to JCPDF card number 37-1492.[39,40] The peak intensities are different from published reports due to quality variation in non-exfoliated bulk MoS_2 powder, as explained from Raman results. Figure 3 indicates successful exfoliation of MoS_2 by S_{Na}CNC and SCNC with a significant difference in the observed diffraction patterns due to a disruption in the layered structure of MoS_2, as shown in Figure 3. The exfoliation of MoS_2 to nanosheets leads to intensity decrease of different planes as well as a corresponding peak broadening, as can be seen in their respective diffractograms. Mostly, exfoliation is confirmed by considering the peak broadening and decrease in the intensity at the peak at 14.4° (002 plane, d—0.61 nm).[36] A similar trend is observed in this work with changes in peak intensity of other peaks MoS_2. This

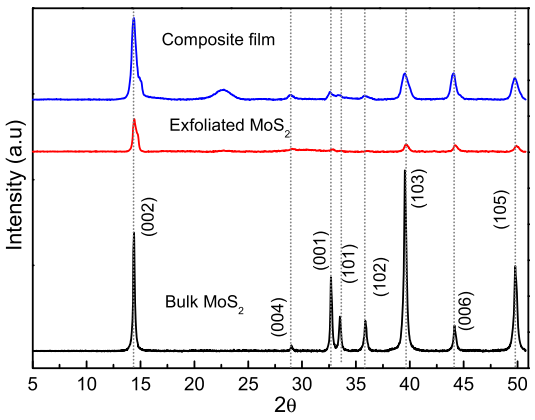

Figure 3. XRD results for bulk MoS_2, exfoliated S_{Na}CNC–MoS_2, and composite film. The XRD pattern for SCNC–MoS_2 is similar to that of S_{Na}CNC–MoS_2.

may be because the MoS_2 nanosheets are formed as few layers or more (see TEM images) rather than monolayers, as described by Li et al.,[34] which is in agreement with the Raman measurements. XRD for CNC samples gave a crystallinity index (CI) of 96% for the SCNC sample and 96.5% for the S_{Na}CNC sample. Cellulose has characteristic peaks at 2θ—14.6° ($1\bar{1}0$ plane), 16.4° (110), 20.6° (012) (amorphous peak), 22.6° (200), and 34.5° (004). From the peaks, areas are calculated (see Figure S5 for CI calculation in Supporting Information).[29,41] CNC samples are more crystalline than the MCC since all amorphous segments present in the cellulose are removed during the acid hydrolysis.[29] Since the amount of CNC used for exfoliating bulk MoS_2 is relatively low, the CNC peaks can hardly be discerned in the diffractograms for exfoliated MoS_2 samples. The peaks correspond to 002 (2θ—14.6°), and the $1\bar{1}0$ (2θ—14.4°) plane is narrower, which may be due to a small contribution (in-plane strain) from CNCs in the peak broadening of exfoliated MoS_2, as CNCs are very rigid. Another peak of cellulose is seen for the composite film, which is discussed in the characterization results of composite films.

The AFM images shown in Figure 4a,b display the small sizes and height profile of CNCs. The low-magnification TEM image of the S_{Na}CNC–MoS_2 shown in Figure 4c,d shows thin flakes of exfoliated MoS_2 nanosheets. The bright and transparent contrast indicates the typical feature shown by thin nanosheet structures. The exfoliation of bulk MoS_2 into 3 or 4 monolayers is displayed in Figure 4d (lines b and c). The high-resolution TEM image shown in Figure 4d shows a d-spacing of ~0.61 nm, in agreement with the XRD results (line a in Figure 4d). Also, the diffraction (SAED) pattern in the inset shows a hexagonal structure, suggesting that the exfoliated nanosheets retain the crystal structure of MoS_2. In the TEM images, the contrast of MoS_2 is stronger due to the higher atom density (heavier atoms) compared to CNCs.

A composite film was prepared using exfoliated MoS_2 nanosheets and S_{Na}CNC to demonstrate its capability as freestanding films having properties that make it suitable for application as an electrode in batteries. The mechanical properties, tensile strength, elongation at break (E %), and elastic modulus of the flexible films consisting of S_{Na}CNC–MoS_2 and MWCNT were measured. Figure 5a displays a stress–strain plot for a strong composite film with strength, E %, and modulus determined to 48 ± 3.2 MPa, 4.2 ± 0.5%, and

https://doi.org/10.1021/acsanm.3c00543
ACS Appl. Nano Mater. 2023, 6, 8270–8278

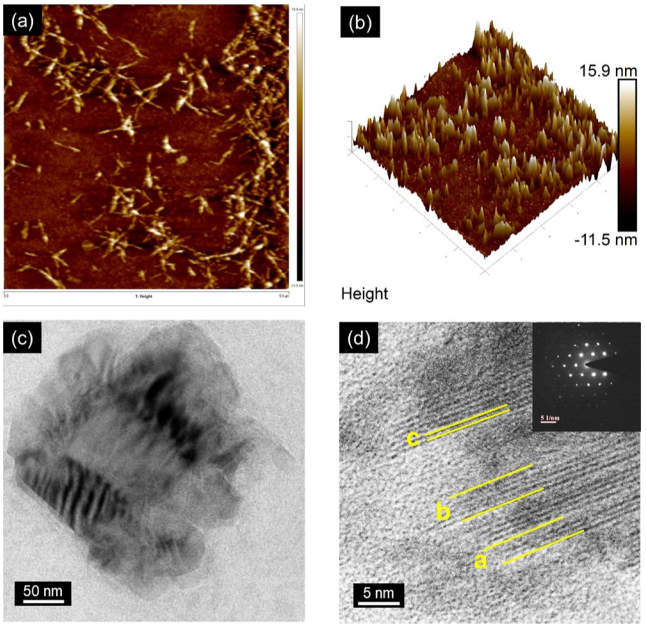

Figure 4. (a) AFM image of SCNC, (b) height profiles of SCNCs, (c) TEM image of S_{Na}CNCMoS_2 nanosheets, and (d) high magnification image of S_{Na}CNCMoS_2 showing the interplanar spacing between layers.

3.8 GPa. In terms of thermal stability [Figure 5b], the film shows good thermal stability with a decomposition temperature of 292 °C. From scanning electron microscopy (SEM) images of the cross-sections of the film (Figure 5c,d), a uniform distribution of components (MoS_2 nanosheets, CNC, and MWCNT) is observed. Also, from the SEM images, it can be concluded that the composite film has a macroporosity throughout the structure and a high structural uniformity. The XRD pattern of composite film is similar to the diffraction patterns observed for exfoliated MoS_2. In addition to characteristic peaks for exfoliated MoS_2, there is a contribution from CNCs in broadening of the peak at 14.6° (002 plane for MoS_2), supporting the interaction of CNCs with the basal plane of MoS_2, as explained in the other studies performed in this work. Also, an additional peak at 22.6° is observed related to the (200) plane of CNCs (Figure S5 in Supporting Information).

As described in the previous section, the composite film shows promising mechanical properties and freestanding film forming ability. These properties make this composite film an attractive material for use as an electrode in battery applications.

Zinc (Zn) batteries are a promising candidate for next-generation rechargeable batteries because of its sustainability, cost, and energy density.[42] However, the deposition of Zn during charge of the battery invariably results in formation and rapid growth of dendrites, manifested in a low Coulombic efficiency and resulting in safety issues.[43] An efficient way to regulate the growth of Zn dendrites is to modify the surface of the substrate for plating to achieve highly reversible plating/stripping of Zn metal on the anode.[44] Herein, we introduced the S_{Na}CNC−MoS_2 film as a substrate [Figure 6a] into a Zn cell and investigated the electrochemical performance of Zn metal plating and stripping. The assembly of the Zn/CNC−MoS_2 cell is shown in Figure 6b. To fully explore the sustainability of Zn battery, an aqueous electrolyte based on $Zn(OAc)_2$ and a cellulose separator (Figure 6c) are used in our work. Therefore, a safe and non-toxic Zn battery can be expected if an appropriate cathode material is added in future work. Stable Zn plating/stripping on the CNC−MoS_2 film was obtained at a current density of 0.5 mA cm^{-2}, as shown in Figure 6d. A small overpotential of 50 mV (Figure 6e) is observed during both Zn plating and stripping processes.

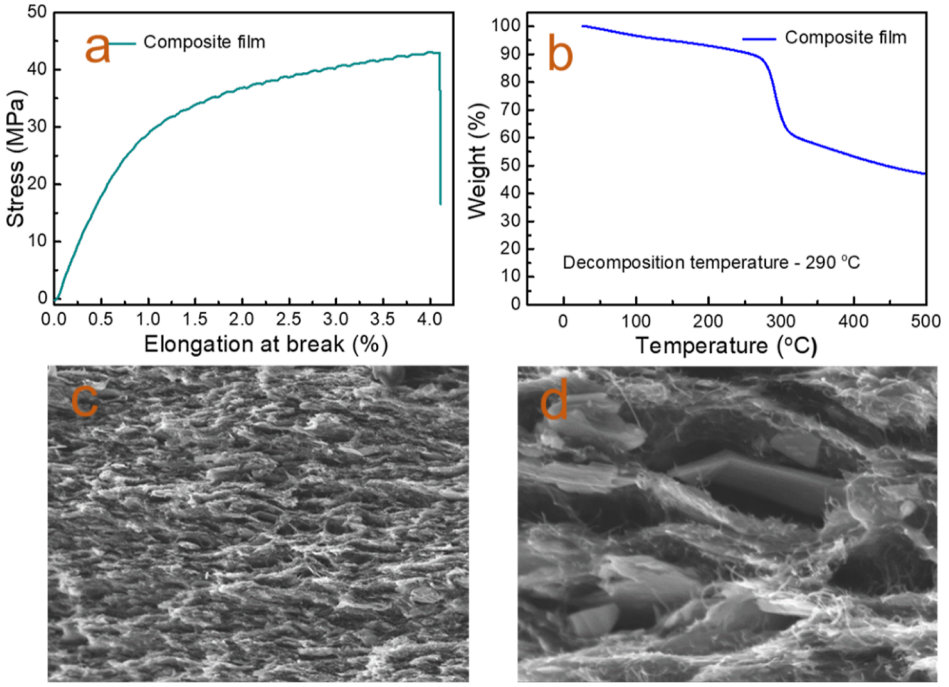

Figure 5. Electrode film: (a) typical stress−strain plot and (b) TGA thermograph and SEM images of the cross-section of the film indicating a distribution of layered material MoS_2 + S_{Na}CNC + MWCNT at (c) 1 μm and (d) 100 nm scale bars.

https://doi.org/10.1021/acsanm.3c00543
ACS Appl. Nano Mater. 2023, 6, 8270−8278

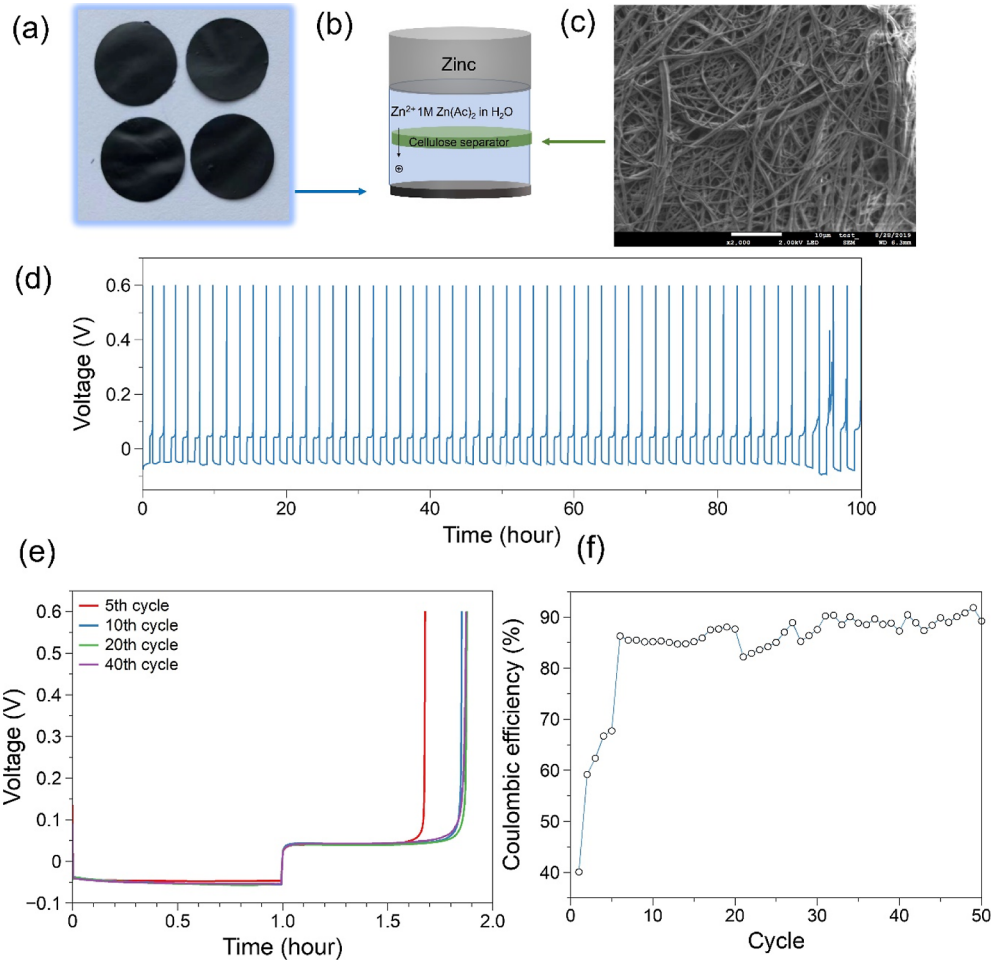

Figure 6. Application of $S_{Na}CNC-MoS_2$ film as a substrate for Zn plating in an aqueous electrolyte. (a) Optical image of $S_{Na}CNC-MoS_2$ film. (b) Assembly of $Zn/S_{Na}CNC-MoS_2$ film half-cell. (c) SEM image of a cellulose separator. (d) Cycling performance of Zn metal in the half-cell under current density of 0.5 mA cm^{-2} for 1 mA h cm^{-2}. (e) Voltage profiles of Zn plating/striping during cycling in 1 M $Zn(Ac)_2$ aqueous electrolyte. (f) Coulombic efficiency of Zn plating/stripping on $S_{Na}CNC-MoS_2$ film.

The low overpotential for Zn plating indicates fast kinetics on the surface of the $CNC-MoS_2$ film, and this may be attributed to fast migration of Zn ions on the MoS_2 nanosheets.[45] In addition, the voltage profiles for the 5th, 20th, and 40th cycle overlap, suggesting the formation of a stable interface between the electrodeposited Zn and the electrolyte and reversible deposition−dissolution reaction at this interface. This allows the Coulombic efficiency of the half-cell to reach 90% after several activation cycles and to be stable for more than 50 cycles. The Coulombic efficiency for the electrochemical plating/stripping of the Zn electrode has been reported as varying from 90 to 99.9% in previous literature,[46] and thus the Coulombic efficiency in this work is not remarkable without full optimization of the electrolyte. This only demonstrates that the $S_{Na}CNC-MoS_2$ film can be potentially introduced as a substrate and be coupled to a Zn cathode to fabricate anode-free Zn batteries with further improvement. The compatibility of the electrolyte with both cathode and anode needs to be explored in addition to improve the Coulombic efficiency of a full cell to a practical level, prior to the realization of this battery concept.

5. CONCLUSIONS

We show that CNCs, obtained by acid hydrolysis of MCC, can be modified to the sodium form of CNCs to demonstrate surfactant-like properties SDS. Sodium sulfated CNCs ($S_{Na}CNC$) are more efficient than other cellulose materials as exfoliating agents to disperse low-cost molybdenum disulfide (MoS_2) powder into MoS_2 nanosheets. The suspensions exhibit good stability, supported by zeta potential measurements. The $S_{Na}CNC-MoS_2$ suspensions have high thermal stability, are neutral, and have long shelf-time. With Raman and XRD, it is observed that CNC interacts with MoS_2, and in the future, solid-state NMR can be used to explain the interfaces between them. $S_{Na}CNC-MoS_2$ suspensions and MWCNTs were combined to fabricate a robust composite film, and it is further explored as an anode substrate in a Zn half-cell, showing a stable electrochemical plating/stripping and the potential to be applied in the green Zn metal batteries. In future studies, the counterion (Na^+) on sulfated CNCs can be exchanged to different alkali counterions (K^+, Li^+, Cs^+, etc.) or other organic counter ionic molecules. Also, it will be promising to explore methodologies that improve the electrochemical performance of the Zn cell with higher Coulombic efficiency.

https://doi.org/10.1021/acsanm.3c00543
ACS Appl. Nano Mater. 2023, 6, 8270−8278

■ ASSOCIATED CONTENT

Supporting Information

The Supporting Information is available free of charge at https://pubs.acs.org/doi/10.1021/acsanm.3c00543.

Characterization of CNC by titration, Fourier transform infrared and TGA, determination of CAC, zeta potential distribution for exfoliated MoS_2 and CNC samples, Raman spectroscopy for SCNC−MoS_2 samples and composite film, XRD for SCNC and S_{Na}CNC samples, and calculation of CI in CNC samples (PDF)

■ AUTHOR INFORMATION

Corresponding Authors

Amit Kumar Sonker − *Department of Chemistry and Chemical Engineering and Wallenberg Wood Science Centre, Chalmers University of Technology, Gothenburg 41296, Sweden; Cellulose Films and Coatings, Biomaterial Processing and Products, VTT Technical Research Centre of Finland Limited, Espoo 02150, Finland;* orcid.org/0000-0003-3825-632X; Email: sonker@chalmers.se, amit.sonker@vtt.fi

Gunnar Westman − *Department of Chemistry and Chemical Engineering and Wallenberg Wood Science Centre, Chalmers University of Technology, Gothenburg 41296, Sweden;* orcid.org/0000-0001-6150-5203; Email: westman@chalmers.se

Authors

Shizhao Xiong − *Department of Physics and Wallenberg Wood Science Centre, Chalmers University of Technology, Gothenburg 41296, Sweden;* orcid.org/0000-0003-1795-7805

Ruchi Aggarwal − *Department of Chemistry, Malaviya National Institute of Technology, Jaipur 302017, India;* orcid.org/0000-0003-0630-3814

Martina Olsson − *Department of Physics, Chalmers University of Technology, Gothenburg 41296, Sweden*

Arnita Spule − *Department of Physics, Chalmers University of Technology, Gothenburg 41296, Sweden*

Seyedehsan Hosseini − *Department of Chemistry and Chemical Engineering, Chalmers University of Technology, Gothenburg 41296, Sweden*

Sumit Kumar Sonkar − *Department of Chemistry, Malaviya National Institute of Technology, Jaipur 302017, India;* orcid.org/0000-0002-2560-835X

Aleksandar Matic − *Department of Physics and Wallenberg Wood Science Centre, Chalmers University of Technology, Gothenburg 41296, Sweden;* orcid.org/0000-0003-4414-9504

Complete contact information is available at: https://pubs.acs.org/10.1021/acsanm.3c00543

Notes

The authors declare no competing financial interest.

■ ACKNOWLEDGMENTS

A.K.S., G.W., A.M., S.X., M.O., A.S., and S.H. thank the Knut and Alice Wallenberg Foundation for financial support. The research has been carried out with the support of Wallenberg Wood Science Center (WWSC). R.A. thanks MNIT Jaipur for the doctoral fellowship, and S.K.S. admires DST-SERB (EEQ/2021/000830) and CSIR [(01(2854)/16/ERMII)] for funding and the Material Research Centre (MRC), MNIT Jaipur.

■ REFERENCES

(1) Chhowalla, M.; Shin, H. S.; Eda, G.; Li, L.-J.; Loh, K. P.; Zhang, H. The Chemistry of Two-Dimensional Layered Transition Metal Dichalcogenide Nanosheets. *Nat. Chem.* **2013**, *5*, 263−275.

(2) Clerici, F.; Fontana, M.; Bianco, S.; Serrapede, M.; Perrucci, F.; Ferrero, S.; Tresso, E.; Lamberti, A. In Situ MoS_2 Decoration of Laser-Induced Graphene as Flexible Supercapacitor Electrodes. *ACS Appl. Mater. Interfaces* **2016**, *8*, 10459−10465.

(3) Saraf, M.; Natarajan, K.; Saini, A. K.; Mobin, S. M. Small Biomolecule Sensors Based on an Innovative MoS_2−RGO Heterostructure Modified Electrode Platform: A Binder-Free Approach. *Dalton Trans.* **2017**, *46*, 15848−15858.

(4) Cao, S.; Shi, L.; Miao, M.; Fang, J.; Zhao, H.; Feng, X. Solution-Processed Flexible Paper-Electrode for Lithium-Ion Batteries Based on MoS_2 Nanosheets Exfoliated with Cellulose Nanofibrils. *Electrochim. Acta* **2019**, *298*, 22−30.

(5) Sabarinathan, M.; Harish, S.; Archana, J.; Navaneethan, M.; Ikeda, H.; Hayakawa, Y. Highly Efficient Visible-Light Photocatalytic Activity of MoS_2−TiO_2 Mixtures Hybrid Photocatalyst and Functional Properties. *RSC Adv.* **2017**, *7*, 24754−24763.

(6) Acerce, M.; Voiry, D.; Chhowalla, M. Metallic 1T Phase MoS_2 Nanosheets as Supercapacitor Electrode Materials. *Nat. Nanotechnol.* **2015**, *10*, 313−318.

(7) Cheng, A.; Zhang, H.; Zhong, W.; Li, Z.; Tang, Y.; Li, Z. Enhanced Electrochemical Properties of Single-Layer MoS_2 Embedded in Carbon Nanofibers by Electrospinning as Anode Materials for Sodium-Ion Batteries. *J. Electroanal. Chem.* **2019**, *843*, 31−36.

(8) Farimani, A. B.; Min, K.; Aluru, N. R. DNA Base Detection Using A Single-Layer MoS_2. *ACS Nano* **2014**, *8*, 7914−7922.

(9) Tang, Q.; Jiang, D.-e. Mechanism of Hydrogen Evolution Reaction on 1T-MoS_2 from First Principles. *ACS Catal.* **2016**, *6*, 4953−4961.

(10) Li, Y.; Yin, X.; Huang, X.; Tian, J.; Wu, W.; Liu, X. The Novel and Facile Preparation of 2DMoS_2@C Composites for Dye Adsorption Application. *Appl. Surf. Sci.* **2019**, *495*, 143626.

(11) Late, D. J.; Liu, B.; Matte, H. S. S. R.; Dravid, V. P.; Rao, C. N. R. Hysteresis In Single-Layer MoS_2 Field Effect Transistors. *ACS Nano* **2012**, *6*, 5635−5641.

(12) Zhang, W.; Cao, Y.; Tian, P.; Guo, F.; Tian, Y.; Zheng, W.; Ji, X.; Liu, J. Soluble, Exfoliated Two-Dimensional Nanosheets as Excellent Aqueous Lubricants. *ACS Appl. Mater. Interfaces* **2016**, *8*, 32440−32449.

(13) Awasthi, G. P.; Kaliannagounder, V. K.; Maharjan, B.; Lee, J. Y.; Park, C. H.; Kim, C. S. Albumin-Induced Exfoliation of Molybdenum Disulfide Nanosheets Incorporated Polycaprolactone/Zein Composite Nanofibers for Bone Tissue Regeneration. *Mater. Sci. Eng., C* **2020**, *116*, 111162.

(14) Li, H.; Wu, J.; Yin, Z.; Zhang, H. Preparation And Applications of Mechanically Exfoliated Single-Layer and Multilayer MoS_2 and WSe_2 Nanosheets. *Acc. Chem. Res.* **2014**, *47*, 1067−1075.

(15) Adilbekova, B.; Lin, Y. B.; Yengel, E.; Faber, H.; Harrison, G.; Firdaus, Y.; El-Labban, A.; Anjum, D. H.; Tung, V.; Anthopoulos, T. D. Liquid Phase Exfoliation of MoS_2 and WS_2 in Aqueous Ammonia and their Application in Highly Efficient Organic Solar Cells. *J. Mater. Chem. C* **2020**, *8*, 5259−5264.

(16) Coleman, J. N.; Lotya, M.; O'Neill, A.; Bergin, S. D.; King, P. J.; Khan, U.; Young, K.; Gaucher, A.; De, S.; Smith, R. J.; Shvets, I. V.; Arora, S. K.; Stanton, G.; Kim, H. Y.; Lee, K.; Kim, G. T.; Duesberg, G. S.; Hallam, T.; Boland, J. J.; Wang, J. J.; Donegan, J. F.; Grunlan, J. C.; Moriarty, G.; Shmeliov, A.; Nicholls, R. J.; Perkins, J. M.; Grieveson, E. M.; Theuwissen, K.; McComb, D. W.; Nellist, P. D.; Nicolosi, V. Two-Dimensional Nanosheets Produced by Liquid Exfoliation of Layered Materials. *Science* **2011**, *331*, 568−571.

(17) O'Neill, A.; Khan, U.; Coleman, J. N. Preparation of High Concentration Dispersions of Exfoliated MoS_2 with Increased Flake Size. *Chem. Mater.* **2012**, *24*, 2414−2421.

(18) Ou, J. Z.; Chrimes, A. F.; Wang, Y.; Tang, S. Y.; Strano, M. S.; Kalantar-zadeh, K. Ion-Driven Photoluminescence Modulation Of Quasi-Two-Dimensional MoS_2 Nanoflakes For Applications In Biological Systems. *Nano Lett.* **2014**, *14*, 857−863.
(19) May, P.; Khan, U.; Hughes, J. M.; Coleman, J. N. Role of Solubility Parameters in Understanding the Steric Stabilization of Exfoliated Two-Dimensional Nanosheets by Adsorbed Polymers. *J. Phys. Chem. C* **2012**, *116*, 11393−11400.
(20) Gupta, A.; Arunachalam, V.; Vasudevan, S. Water Dispersible, Positively and Negatively Charged MoS_2 Nanosheets: Surface Chemistry and the Role of Surfactant Binding. *J. Phys. Chem. Lett.* **2015**, *6*, 739−744.
(21) Smith, R. J.; King, P. J.; Lotya, M.; Wirtz, C.; Khan, U.; De, S.; O'Neill, A.; Duesberg, G. S.; Grunlan, J. C.; Moriarty, G.; Chen, J.; Wang, J.; Minett, A. I.; Nicolosi, V.; Coleman, J. N. Large-Scale Exfoliation of Inorganic Layered Compounds in Aqueous Surfactant Solutions. *Adv. Mater.* **2011**, *23*, 3944−3948.
(22) Ma, H.; Shen, Z. G.; Ben, S. Surfactant-Free Exfoliation of Multilayer Molybdenum Disulfide Nanosheets in Water. *J. Colloid Interface Sci.* **2019**, *537*, 28−33.
(23) Liu, X. Y.; Chen, H.; Lin, J.; Li, Y.; Guo, L. Q. Exfoliation of Transition-Metal Dichalcogenides using ATP in Aqueous Solution. *Chem. Commun.* **2019**, *55*, 2972−2975.
(24) Liu, W. S.; Zhao, C. Y.; Zhou, R.; Zhou, D.; Liu, Z. L.; Lu, X. H. Lignin-Assisted Exfoliation of Molybdenum Disulfide in Aqueous Media and its Application in Lithium Ion Batteries. *Nanoscale* **2015**, *7*, 9919−9926.
(25) Deng, R.; Yi, H.; Fan, F. Y.; Fu, L.; Zeng, Y.; Wang, Y.; Li, Y. C.; Liu, Y. L.; Ji, S. J.; Su, Y. Facile Exfoliation of MoS_2 Nanosheets By Protein as a Photothermal-Triggered Drug Delivery System for Synergistic Tumor Therapy. *RSC Adv.* **2016**, *6*, 77083−77092.
(26) Li, Y.; Zhu, H.; Shen, F.; Wan, J.; Lacey, S.; Fang, Z.; Dai, H.; Hu, L. Nanocellulose As Green Dispersant for Two-Dimensional Energy Materials. *Nano Energy* **2015**, *13*, 346−354.
(27) Yang, L.; Mukhopadhyay, A.; Jiao, Y.; Yong, Q.; Chen, L.; Xing, Y.; Hamel, J.; Zhu, H. Ultralight, Highly Thermally Insulating and Fire Resistant Aerogel by Encapsulating Cellulose Nanofibers with Two-Dimensional MoS_2. *Nanoscale* **2017**, *9*, 11452−11462.
(28) Sahlin, K.; Forsgren, L.; Moberg, T.; Bernin, D.; Rigdahl, M.; Westman, G. Surface Treatment of Cellulose Nanocrystals (CNC): Effects on Dispersion Rheology. *Cellulose* **2018**, *25*, 331−345.
(29) Aggarwal, R.; Garg, A. K.; Saini, D.; Sonkar, S. K.; Sonker, A. K.; Westman, G. Cellulose Nanocrystals Derived from Microcrystalline Cellulose for Selective Removal of Janus Green Azo Dye. *Ind. Eng. Chem. Res.* **2023**, *62*, 649−659.
(30) Scholz, N.; Behnke, T.; Resch-Genger, U. Determination of the Critical Micelle Concentration of Neutral and Ionic Surfactants with Fluorometry, Conductometry, and Surface Tension—A Method Comparison. *J. Fluoresc.* **2018**, *28*, 465−476.
(31) Dominguez, A.; Fernandez, A.; Gonzalez, N.; Iglesias, E.; Montenegro, L. Determination of Critical Micelle Concentration of Some Surfactants by Three Techniques. *J. Chem. Educ.* **1997**, *74*, 1227.
(32) Beck, S.; Bouchard, J. Auto-Catalyzed Acidic Desulfation of Cellulose Nanocrystals. *Nord. Pulp Pap. Res. J.* **2014**, *29*, 6−14.
(33) Tang, C.; Spinney, S.; Shi, Z.; Tang, J.; Peng, B.; Luo, J.; Tam, K. C. Amphiphilic Cellulose Nanocrystals for Enhanced Pickering Emulsion Stabilization. *Langmuir* **2018**, *34*, 12897−12905.
(34) Li, H.; Zhang, Q.; Yap, C. C. R.; Tay, B. K.; Edwin, T. H. T.; Olivier, A.; Baillargeat, D. From Bulk to Monolayer MoS_2: Evolution of Raman Scattering. *Adv. Funct. Mater.* **2012**, *22*, 1385−1390.
(35) Van Thanh, D.; Pan, C.-C.; Chu, C.-W.; Wei, K.-H. Production of Few-Layer MoS_2 Nanosheets through Exfoliation of Liquid N_2−Quenched Bulk MoS_2. *RSC Adv.* **2014**, *4*, 15586−15589.
(36) Zhu, J. Y.; Wang, H.; Liu, J. W.; Ouyang, L. Z.; Zhu, M. Exfoliation of MoS_2 and h-Bn Nanosheets by Hydrolysis of $LiBH_4$. *Nanotechnology* **2017**, *28*, 115604.
(37) Lee, C.; Yan, H.; Brus, L. E.; Heinz, T. F.; Hone, J.; Ryu, S. Anomalous Lattice Vibrations of Single- and Few-Layer MoS_2. *ACS Nano* **2010**, *4*, 2695−2700.
(38) Windom, B. C.; Sawyer, W. G.; Hahn, D. W. A Raman Spectroscopic Study Of MoS_2 And MoO_3: Applications to Tribological Systems. *Tribol. Lett.* **2011**, *42*, 301−310.
(39) Yang, L.; Cui, X.; Zhang, J.; Wang, K.; Shen, M.; Zeng, S.; Dayeh, S. A.; Feng, L.; Xiang, B. Lattice Strain Effects on the Optical Properties of MoS_2 Nanosheets. *Sci. Rep.* **2014**, *4*, 5649.
(40) Gao, D. Q.; Si, M. S.; Li, J. Y.; Zhang, J.; Zhang, Z. P.; Yang, Z. L.; Xue, D. S. Ferromagnetism in Freestanding MoS_2 Nanosheets. *Nanoscale Res. Lett.* **2013**, *8*, 129.
(41) Daicho, K.; Saito, T.; Fujisawa, S.; Isogai, A. The Crystallinity of Nanocellulose: Dispersion-Induced Disordering of the Grain Boundary in Biologically Structured Cellulose. *ACS Appl. Nano Mater.* **2018**, *1*, 5774−5785.
(42) Service, R. F. Zinc Aims to Beat Lithium Batteries at Storing Energy. *Science* **2021**, *372*, 890−891.
(43) Wang, F.; Borodin, O.; Gao, T.; Fan, X.; Sun, W.; Han, F.; Faraone, A.; Dura, J. A.; Xu, K.; Wang, C. Highly Reversible Zinc Metal Anode for Aqueous Batteries. *Nat. Mater.* **2018**, *17*, 543−549.
(44) Zheng, J.; Zhao, Q.; Tang, T.; Yin, J.; Quilty, C. D.; Renderos, G. D.; Liu, X.; Deng, Y.; Wang, L.; Bock, D. C.; et al. Reversible Epitaxial Electrodeposition of Metals in Battery Anodes. *Science* **2019**, *366*, 645−648.
(45) Yuan, C.; Yin, L.; Du, P.; Yu, Y.; Zhang, K.; Ren, X.; Zhan, X.; Gao, S. Microgroove-Patterned Zn Metal Anode Enables Ultra-Stable and Low-Overpotential Zn Deposition for Long-Cycling Aqueous Batteries. *Chem. Eng. J.* **2022**, *442*, 136231.
(46) Ma, L.; Schroeder, M. A.; Borodin, O.; Pollard, T. P.; Ding, M. S.; Wang, C.; Xu, K. Realizing High Zinc Reversibility in Rechargeable Batteries. *Nat. Energy* **2020**, *5*, 743−749.

https://doi.org/10.1021/acsanm.3c00543
ACS Appl. Nano Mater. 2023, 6, 8270−8278